

Ultraviolet detectors for astrophysics missions: A case study with the Star-Planet Activity Research CubeSat (SPARCS)

April Jewell,^{1*} John Hennessy,¹ Todd Jones,¹ Samuel Cheng,¹ Alexander Carver,¹ David Ardila,¹ Evgenya Shkolnik,² Michael Hoenk,¹ and Shouleh Nikzad¹

¹Jet Propulsion Laboratory, California Institute of Technology, Pasadena, CA 91109

²School for Earth and Space Exploration, Arizona State University, Tempe, AZ 85281

ABSTRACT

Here we discuss high-performance UV detectors to be used with the planned Star-Planet Activity Research CubeSat (SPARCS). SPARCS is a 6U cubesat designed to monitor M stars (0.1 – 0.6 solar masses) in two photometric bands in the near UV and far UV (S-NUV, 260-300 nm; S-FUV, 150-170 nm). SPARCS targets range in mass and age, including young stars (10-20 Myr), which are likely forming terrestrial planets, to old stars with known transiting planets, allowing us to map the evolution of UV emission and flare rates. The spectral slope, variability and evolution of a host star's high-energy radiation would provide realistic input stellar fluxes to planet atmospheric models, which would aid in understanding the evolution and habitability of a planet and in interpreting its transmission and emission spectrum.

The baseline S-NUV detector is a 2D-doped (delta-doped or superlattice-doped) charge coupled device (CCD) optimized with a custom antireflection (AR) coating to achieve quantum efficiency (QE)>70% throughout the S-NUV band. The S-NUV detector would be coupled with a stand-alone red-blocking filter that provides at least three orders of magnitude (i.e., \geq OD3) out-of-band suppression, critical for the observations of such cool, red stars. Their combined throughput would be >25% (peak) in the S-NUV. The baseline S-FUV detector is a 2D-doped CCD optimized for the S-FUV band; it includes an integrated filter designed to maximize in-band throughput with good red-leak suppression. As designed, the solar-blind silicon detector achieves peak QE>35% in the S-FUV band and \geq OD2 out-of-band suppression. SPARCS has baselined a dichroic design that allows for simultaneous S-NUV and S-FUV observation.

SPARCS would advance 2D-doped detectors and detector-integrated out-of-band-rejection filter technologies for their potential application in future mission concepts such as LUVOIR and HabEx.

Keywords: SPARCS, SPARCam, delta-doped, 2D-doped, superlattice-doped, solar-blind silicon, ultraviolet, cubesat

*april.d.jewell@jpl.nasa.gov

1. INTRODUCTION

M dwarfs are the most common of planet hosts in our galaxy with roughly 40 billion terrestrial planets in the habitable zone (HZ).^{1,2} M dwarfs are known to stay active with high emission levels and frequent flares throughout their lives.³ UV flux during the super-luminous, pre-main sequence phase of M stars drives water loss and photochemical O₂ buildup for terrestrial planets within the HZ.⁴ The planet's UV environment will also affect its atmospheric composition and its potential for habitability and the corresponding detectability of biosignatures (Figure 1). In depth characterization of the UV environments of M dwarf planets will be crucial to understanding these parameters and aid in discriminating between biological and abiotic sources for observed biosignatures.

The NASA-funded Star-Planet Activity Research CubeSat (SPARCS) observatory would be the first mission to provide the spectral slope, flux and evolution of M dwarf stellar UV radiation on time-scales from minutes to weeks. SPARCS, led by Arizona State University (PI Evgenya Shkolnik), would be a 6U cubesat with two UV channels to monitor ~20 of

these low-mass stars. The SPARCS near UV (S-NUV) bandpass spans 260-300 nm with its strongest feature being the upper-chromospheric Mg II doublet (280 nm) formed at $\sim 10^4$ K, similar to, and known to correlate with, Lyman- α (121.5 nm).⁵ The SPARCS far UV (S-FUV) bandpass spans 150-170 nm, and includes the C IV doublet (155 nm), formed in the transition region at $\sim 10^5$ K, and the He II line (164 nm), formed in the corona at $\sim 10^7$ K. The UV emission probed by SPARCS can photodissociate important diagnostic molecules in a planetary atmosphere, such as water (H₂O), ozone (O₃), sulfur dioxide (SO₂), a signature of volcanic activity, and ammonia (NH₃), an important source of the nitrogen required to build amino acids. SPARCS has baselined a dichroic design that would allow for simultaneous S-NUV and S-FUV observation; the crossover wavelength for the dichroic would be at 233 ± 5 nm.

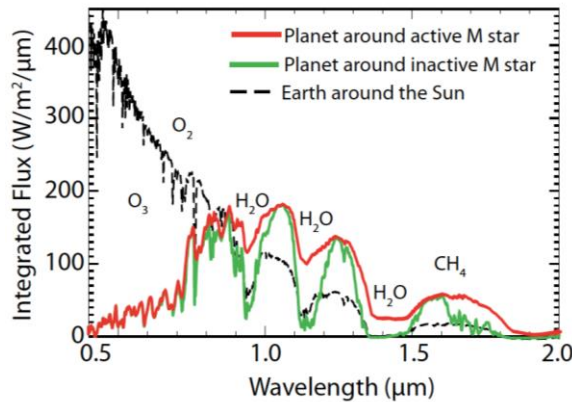


Figure 1. The stellar UV flux has a dramatic effect on a planet’s detected atmospheric content. The plot shows an Earth-like planet spectrum in the HZ of an active (red) and inactive (green) M4 dwarf. The spectrum of the Earth around the Sun is shown black for comparison. (Adapted from Rugheimer et al.⁶)

For each of its targets SPARCS would conduct nearly continuous observations for one to three complete stellar rotations (4–45 days) over a mission lifetime of two years. This represents an increase in M dwarf UV measurements from timescales measured in minutes—e.g. with Hubble Space Telescope (*HST*) and the Galaxy Evolution Explorer (*GALEX*)—to weeks, allowing SPARCS to capture short-term flaring and long-term rotational modulation (Figure 2). These dedicated, prolonged observations are required to develop the statistics needed to constrain input parameters for photochemical atmosphere models.

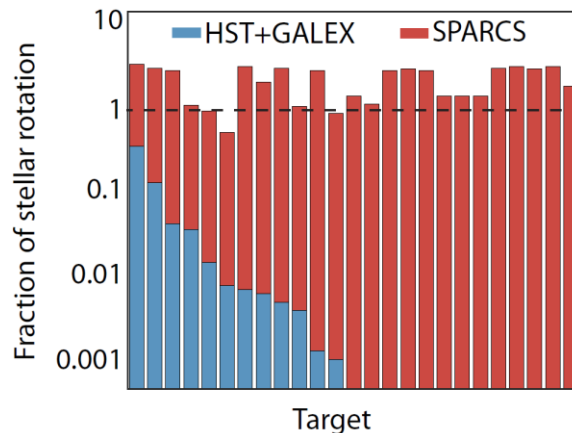


Figure 2. SPARCS would provide three orders of magnitude increase in M dwarf UV measurements over the total UV data collected with *HST* and *GALEX*. SPARCS would observe on timescales from minutes to weeks, recording short-term flaring and longer-term rotational modulation.

2. SPARCS ULTRAVIOLET DETECTORS

The SPARCS camera (SPARCam) advances UV detector technology by flying high QE, UV-optimized detectors and detector-integrated out-of-band-rejection filters developed at JPL. JPL's UV detector technologies are based on nanoscale engineering processes, including delta- and superlattice-doping ("2D-doping") and atomic layer deposition (ALD).⁷⁻⁹ Our detectors have previously been demonstrated in the laboratory environment, in ground-based systems, and on sub-orbital payloads.¹⁰ This manuscript provides the details of the SPARCS detectors, which would be produced using JPL's established and proven 2D-doping and UV bandpass filter technologies.¹⁰⁻¹² An in depth discussion of the SPARCS mission and complete payload are the subject of an accompanying proceedings manuscript.¹³

2.1 SPARCam NUV Channel

The baseline S-NUV detector is a 2D-doped, AR-coated, 1k x 1k (1k x 2k, frame transfer), 13 μm CCD47-20 (Teledyne-e2v). The model response of detector is shown in Figure 3 along with the measured response of a prototype detector. The prototype detector included a simple, single layer hafnium oxide (HfO_2) AR coating, resulting in $\text{QE} > 70\%$ at the S-NUV band center.¹⁰ The same processes used to produce this performance would be applied to the SPARCS detector.

The HfO_2 AR coating to be used with the S-NUV detector has been proven to improve detector response in the S-NUV band. However, suppression of out-of-band light is also desired for SPARCS, as the faint UV signals expected may be hindered by inadequate rejection of stellar emission in the visible and near infrared regions of the spectrum. The "red-leak" will mask the UV signal if filtering is not adequate. Thus, SPARCam would employ a stand-alone, commercial filter for red-leak suppression in the S-NUV channel. Together with the 2D-doped CCD, the filter would define the NUV channel bandwidth and in-band throughput. The filter would also provide red-leak suppression of three- to four-orders of magnitude out to 1000 nm where silicon becomes transparent. The expected throughput of the S-NUV channel is shown in Figure 4; the full width half maximum (FWHM) peak would span 260-300 nm with maximum transmission $\sim 30\%$.

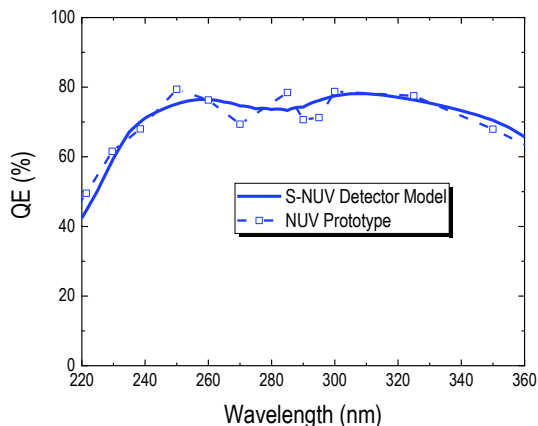


Figure 3. Model performance (solid line) of the baseline S-NUV detector is compared to the measured performance (dashed line, open markers) of a prototype detector in the same wavelength range.¹⁰ The prototype detector data was corrected for quantum yield using correction factors derived by Kuschneres et al.¹⁴

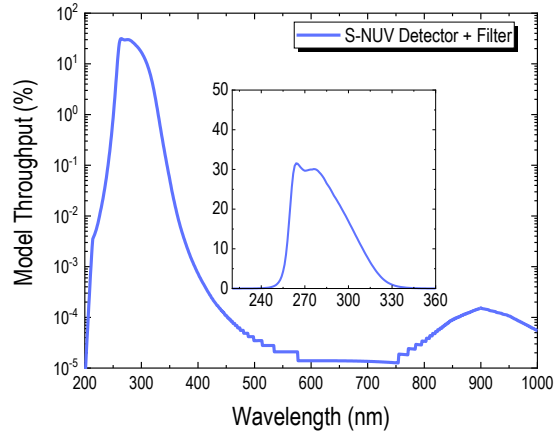


Figure 4. Model throughput of the S-NUV channel defined by the combined throughput of the baseline 2D-doped, AR coated detector together with a commercial bandpass filter. Inset shows the expected bandpass throughput on a linear scale.

2.2 SPARCam FUV Channel

The baseline S-FUV detector is also a 2D-doped CCD; rather than a simple AR coating, the S-FUV detector would include an integrated metal dielectric filter (MDF). The integrated filter would perform a similar function as the stand-alone, commercial filter in the S-NUV channel; it would define the FUV bandpass and provide good red-leak suppression out to 1000 nm. The S-FUV MDF structure will be adapted from a design JPL previously developed for use with silicon APDs.^{15,16} These filters were based on three- and five-layer Al/Al₂O₃ filter stacks optimized for the 200-240 nm bandpass with two- to three-orders of red-leak suppression. Al₂O₃ is not an appropriate material selection for the S-FUV bandpass, as it exhibits strong absorption at wavelengths less than ~190 nm. As such, the SPARCS baseline design uses a MDF with an Al/AlF₃ stack using processes already developed at JPL; the model throughput of the S-FUV channel is shown in Figure 5. When integrated with the 2D-doped detector, the seven-layer Al/AlF₃ MDF is designed to yield peak QE > 35% and a red-leak suppression of more than two orders of magnitude out to 1000 nm. The SPARCS dichroic filter would provide additional red-leak suppression in the S-FUV bandpass.¹³

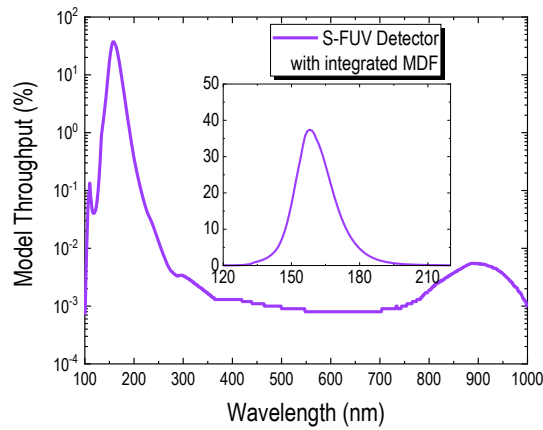


Figure 5. Model performance of the baseline S-FUV 2D-doped detector with integrated MDF. Inset shows the expected bandpass throughput on a linear scale.

Development of the MDF for the S-FUV detector is on-going; we have demonstrated deposition of FUV-optimized MDFs on non-functional prototype devices with the same dimensions as the baseline SPARCS devices (Figure 6). Five-layer Al/AlF₃ MDFs were deposited with well-defined spatial boundaries, preventing interference with the device's bond pads. Reflectance measurements from two different systems show that the film's optical properties are as expected, exhibiting two orders of magnitude out-of-band suppression.

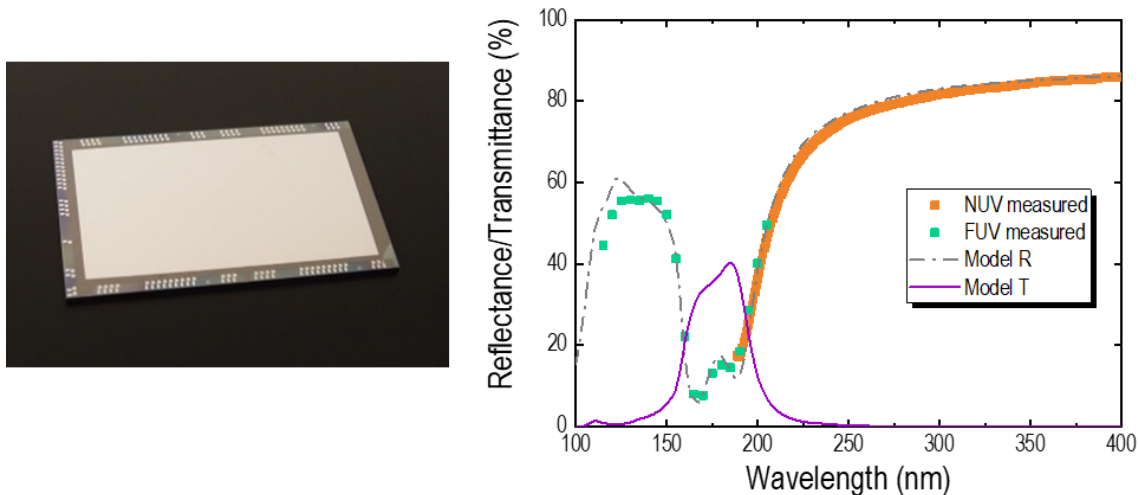


Figure 6. (left) Non-functional prototype device with an integrated, five-layer, Al/AlF₃ MDF. (right) Reflectance measurement from the sample on the left showing good agreement with the model.¹⁶

JPL'S BACKSIDE PROCESSES

2.3 Two-dimensional Doping

By using silicon-based detectors, the astrophysics community is able to take advantage of the enormous investment made in the silicon industry. As measurement requirements become more demanding, large format, high performance imaging arrays will offer important advantages for the future of space exploration as well as the semiconductor and medical industries. A key performance metric and challenge for scientific imagers is photometric stability, a parameter that depends largely on passivation at the detector interface. Without passivation, defects at the Si/SiO₂ interface result in dynamic surface charging and trapping effects that lead to QE hysteresis and persistence. Such behavior would be detrimental to missions such as SPARCS that are directly probing sources with time-variable emissions.

JPL's delta- and superlattice-doping ("2D-doping") processes use low temperature molecular beam epitaxy (MBE) to embed an atomically-thin (2D), highly concentrated layer of dopant atoms within a few nm of the surface.⁷ This high precision growth technique allows for nanometer-scale control over dopant distribution and near-surface band structure. The 2D-doped layer forms a nanometer-scale surface potential barrier that isolates the detector from Si/SiO₂ interface traps, resulting in exceptional stability for 2D-doped arrays, while quantum confinement and ballistic transport effects minimize trapping and recombination, ensuring high QE throughout the challenging NUV and FUV bands. Furthermore, because it is a low temperature process, JPL's 2D-doping is compatible as a post-fabrication step that does not damage existing device structures (polysilicon gates, metals, and oxide layers that comprise the frontside CCD detector electronics). Our processes are also applicable to virtually any silicon-based photodetector, and have been demonstrated with CCDs, complementary metal-oxide-semiconductor active pixel sensors (CMOS APS), avalanche photodiodes (APDs), and silicon PIN diode arrays.^{7,10,17-24}

2.4 Atomic Layer Deposition based Antireflection Coatings

Ideal AR coatings are uniform, pinhole free and reproducible; at JPL we use atomic layer deposition (ALD) for the majority of our filters and AR coatings. ALD is a technique whereby thin films are grown through a series of self-limiting chemical reactions at a substrate surface. It has been widely used for the preparation of dielectric materials, including metal oxides,²⁵⁻²⁸ metal fluorides,²⁹⁻³² and metal nitrides, as well as thin metal films and nanoparticles.³³ Due to its highly controlled growth mechanism, in which a film is deposited a fraction of a monolayer at a time, ALD offers nanometer-scale control over film thickness and composition with well-defined, sharp interfaces.^{9,34} These characteristics make ALD ideally suited for precision processing of scientific imagers where even slight non-uniformities in detector sensitivity can diminish science return.

The effectiveness of ALD-based AR coatings for improving silicon photodetector response is well-established. Early work with single layer metal oxide coatings at JPL led to world record QE in narrow bandpass regions throughout the 100-300 nm wavelength range.³⁵ We have since extended our work to multilayer AR coatings for both broadband and narrow band applications. For example, JPL recently delivered multiple 2D-doped detectors for the facilities at Caltech Optical Observatories, including WaSP (Wafer-Scale imager for Prime) and ZTF (Zwicky Transient Facility). Multilayer AR coatings optimized for 320-1000 nm were applied to deep depletion CCDs resulting in average QE>80% throughout this wavelength range.^{9,10} Similarly, JPL delivered the UV detector for the Faint Intergalactic Red-shifted Emission Balloon (FIREBall-2) experiment; multilayer AR coatings were optimized for the UV stratospheric balloon window spanning ~195 to 225 nm. These coatings were applied to electron multiplying CCDs (EMCCDs), resulting in QE≈80% for the FIREBall-2 detector prototypes.³⁶⁻³⁸ The materials and processes developed in these and other projects will be used for the SPARCS detector.

2.5 Integrated MDFs for Solar-blind Silicon

Antireflection coatings such as those described in the previous section have been widely-used for improving detector response in a given bandpass, and they can be optimized for both broadband and narrow band performance. However, there are cases, such as SPARCS, for which suppression of out-of-band light is also desired. When paired with 2D-doped arrays, JPL's integrated MDFs achieve stable UV response together with the necessary red-leak suppression. These MDFs are essentially Fabry-Pérot filters, which have a long history of use as stand-alone bandpass filters deposited on transparent substrates. The basic concept of an MDF consists of depositing matched parallel reflecting metal layers separated by a transparent spacer layer in order to destructively phase-match the reflection from the metal layer at a particular wavelength and maximize transmission through the structure. Out-of-band light is not subjected to the same interference and is rejected by the high natural reflectance of the stack. Compared to in-line filters prepared on transparent substrates, detector integrated MDFs allow for index matching and higher in band throughput.³⁹

3. MODELS

The optical models presented in this paper were developed using the transfer matrix method and the TFCalc software package.⁴⁰ Optical constants for silicon, aluminum, and various metal oxides and metal fluorides were taken from Palik and the Sopra database.^{40,41} It is well known that a material's optical properties can vary depending on the deposition method; thus spectroscopic ellipsometry data collected using laboratory prepared samples (Horiba UVISEL 2; J. A. Woollam VUV-VASE) were also used in modeling where appropriate.

4. ACKNOWLEDGEMENTS

The research described in this paper was carried out in part at the Jet Propulsion Laboratory, California Institute of Technology, under a contract with the National Aeronautics and Space Administration. We thank the SPARCS team for their valuable input. The information provided about SPARCS is pre-decisional and is provided for planning and discussion purposes only.

REFERENCES

- [1] Dressing, C. D., Charbonneau, D., "The Occurrence of Potentially Habitable Planets Orbiting M Dwarfs Estimated from the Full Kepler Dataset and an Empirical Measurement of the Detection Sensitivity," arXiv: astro-ph.EP **1501.01623** (2015).
- [2] Bochanski, J. J., Hawley, S. L., Covey, K. R., West, A. A., Reid, I. N., Golimowski, D. A., Ivezić, Z., "The Luminosity and Mass Functions of Low-Mass Stars in the Galactic Disk: II. The Field," 2679–2699 (2010).
- [3] Shkolnik, E. L., Barman, T. S., "Hazmat. I. The evolution of far-UV and near-UV emission from early M stars," *Astron. J.* **148**(4) (2014).
- [4] Luger, R., Barnes, R., "Extreme Water Loss and Abiotic O₂ Buildup on Planets Throughout the Habitable Zones of M Dwarfs," *Astrobiology* **15**(2), 119–143 (2015).
- [5] Linsky, J. L., France, K., Ayres, T., "COMPUTING INTRINSIC LY α FLUXES OF F5 V TO M5 V STARS," *Astrophys. J.* **766**(2), 69 (2013).

- [6] Rugheimer, S., Kaltenecker, L., Segura, A., Linsky, J., Mohanty, S., “EFFECT OF UV RADIATION ON THE SPECTRAL FINGERPRINTS OF EARTH-LIKE PLANETS ORBITING M STARS,” *Astrophys. J.* **809**(1), 57, IOP Publishing (2015).
- [7] Hoenk, M. E., Grunthaner, P. J., Grunthaner, F. J., Terhune, R. W., Fattahi, M., Tseng, H.-F., “Growth of a delta-doped silicon layer by molecular beam epitaxy on a charge-coupled device for reflection-limited ultraviolet quantum efficiency,” *Appl. Phys. Lett.* **61**(9), 1084–1086 (1992).
- [8] Hoenk, M. E., Carver, A. G., Jones, T. J., Dickie, M. R., Sgro, J., Tsur, S., “Superlattice-doped Imaging Detectors: Structure, Physics and Performance,” *Sci. Detect. Work.*, Florence (2013).
- [9] Jewell, A. D., Hennessy, J., Hoenk, M. E., Nikzad, S., “Wide band antireflection coatings deposited by atomic layer deposition,” *Proc. SPIE - Int. Soc. Opt. Eng.* **8820** (2013).
- [10] Nikzad, S., Jewell, A. D., Hoenk, M. E., Jones, T. J., Hennessy, J., Goodsall, T., Carver, A. G., Shapiro, C., Cheng, S. R., et al., “High-efficiency UV/optical/NIR detectors for large aperture telescopes and UV explorer missions: development of and field observations with delta-doped arrays,” *J. Astron. Telesc. Instruments, Syst.* **3**(03), 1 (2017).
- [11] Nikzad, S., Hoenk, M. E., Hennessy, J., Jewell, A. D., Carver, A. G., Jones, T. J., Cheng, S. L., Goodsall, T., Shapiro, C., “High performance silicon imaging arrays for cosmology, planetary sciences, & other applications,” *Tech. Dig. - Int. Electron Devices Meet. IEDM 2015–Febru*(February) (2015).
- [12] Nikzad, S., Hoenk, M., Jewell, A. D., Hennessy, J. J., Carver, A. G., Jones, T. J., Goodsall, T. M., Hamden, E. T., Suvarna, P., et al., “Single photon counting UV solar-blind detectors using silicon and III-nitride materials,” *Sensors* **16**(6) (2016).
- [13] Scowen, P. A., Shkolnik, E., Ardila, D., Bowman, J., Jacobs, D., Jewell, A., Beasley, M., Barman, T., Gorjian, V., et al., “Monitoring the high-energy radiation environment of exoplanets around low-mass stars with SPARCS (star-planet activity research CubeSat),” *Proc. SPIE 10699 Sp. Telesc. Instrum. 2018 Ultrav. to Gamma Ray, J.-W. A. Den Herder, S. Nikzad, and K. Nakazawa, Eds.*, 10699:14, Austin, TX (2018).
- [14] Kuschnerus, P., Rabus, H., Richter, M., Scholze, F., Werner, L., Ulm, G., “Characterization of photodiodes as transfer detector standards in the 120 nm to 600 nm spectral range,” *Metrologia* **35**(4), 355–362 (2003).
- [15] Hitlin, D. D. G., Kim, J. H. J. H., Trevor, J., Hoenk, M., Hennessy, J., Jewell, A., Farrell, R., McClish, M., Hoenk, M., et al., “An APD for the Detection of the Fast Scintillation Component of BaF₂,” *IEEE Trans. Nucl. Sci.* **63**(2), 513–515 (2016).
- [16] Hennessy, J., Jewell, A. D., Hoenk, M. E., Hitlin, D., McClish, M., Carver, A. G., Jones, T. J., Nikzad, S., “Materials and process development for the fabrication of far ultraviolet device-integrated filters for visible-blind Si sensors,” *Proc. SPIE 10209 Image Sens. Technol. Mater. Devices, Syst. Appl. IV* **10209**, 102090P:9 (2017).
- [17] Hoenk, M. E., Grunthaner, P. J., Grunthaner, F. J., Terhune, R. W., Fattahi, M. M., “Epitaxial Growth of p+ Silicon on a Backside-thinned CCD for Enhanced UV Response,” *Proc. SPIE 1656, High-Resolution Sensors Hybrid Syst.* **1656**(1992), M. M. Blouke, W. Chang, L. J. Thorpe, and R. P. Khosla, Eds., 488–496, San Jose, CA, USA (1992).
- [18] Nikzad, S., Hoenk, M. E., Grunthaner, P. J., Terhune, R. W., Grunthaner, F. J., Winzenread, R., Fattahi, M., “Delta-doped CCDs for Enhanced UV Performance,” 138–146 (1994).
- [19] Nikzad, S., Jones, T. J., Elliott, S. T., Cunningham, T. J., Deelman, P. W., Walker, A. B. C., Oluseyi, H. M., “Ultrastable and uniform EUV and UV detectors,” *Proc. SPIE 4139, Instrum. UV/EUV Astron. Sol. Mission.* **4139**, S. Fineschi, C. M. Korendyke, O. H. W. Siegmund, and B. E. Woodgate, Eds., 250–258, San Diego, CA, USA (2000).
- [20] Deelman, P. W., Nikzad, S., Blouke, M. M., “Delta-doped CCDs with integrated UV coatings,” *Proc. SPIE 3965, Sensors Camera Syst. Sci. Ind. Digit. Photography Appl.* **3965**, M. M. Blouke, N. Sampat, G. M. J. Williams, and T. Yeh, Eds., 462–466, San Jose, CA, USA (2000).
- [21] Nikzad, S., Cunningham, T. J., Hoenk, M. E., Ruiz, R. P., Soules, D. M., Holland, S. E., “Direct detection of 0.1–20 keV electrons with delta doped, fully depleted, high purity silicon p-i-n diode arrays,” *Appl. Phys. Lett.* **89**(18), 182114 (2006).
- [22] Hoenk, M. E., Jones, T. J., Dickie, M. R., Greer, F., Cunningham, T. J., Blazejewski, E. R., Nikzad, S., “Delta-doped Back-illuminated CMOS Imaging Arrays: Progress and Prospects,” *Proc. SPIE 7419, Infrared Syst. Photoelectron. Technol. IV* **7419**, E. L. Dereniak, J. P. Hartke, P. D. LeVan, R. E. Longshore, and A. K. Sood, Eds., OT:15, San Diego, CA, USA (2009).
- [23] Hoenk, M. E., Carver, A. G., Jones, T. J., Dickie, M., Cheng, P., Greer, F., Nikzad, S., Sgro, J., Tsur, S., “The

- DUV Stability of Superlattice-doped CMOS Detector Arrays,” *Int. Image Sens. Work.*, Snowbird, UT, USA (2013).
- [24] Hoenk, M. E., Nikzad, S., Carver, A. G. A. G., Jones, T. J. T. J., Hennessy, J. J., Jewell, A. D., Sgro, J., Tsur, S., McClish, M., et al., “Superlattice-doped silicon detectors: progress and prospects,” *Proc. SPIE 9154*, High Energy, Opt. Infrared Detect. Astron. VI **9154**, A. D. Holland and J. Beletic, Eds., 915413, Montreal, CA (2014).
- [25] van Hemmen, J. L., Heil, S. B. S., Klootwijk, J. H., Roozeboom, F., Hodson, C. J., van de Sanden, M. C. M., Kessels, W. M. M., “Plasma and Thermal ALD of Al₂O₃ in a Commercial 200 mm ALD Reactor,” *J. Electrochem. Soc.* **154**(7), G165 (2007).
- [26] Dingemans, G., van Helvoirt, A. A., van de Sanden, M. C. M., Kessels, W. M. M., “Plasma-Assisted Atomic Layer Deposition of Low Temperature SiO₂,” *ECS Trans.* **35**(4), 191–204 (2011).
- [27] Liu, X., Ramanathan, S., Longdergan, A., Srivastava, A., Lee, E., Seidel, T. E., Barton, J. T., Pang, D., Gordon, R. G., “ALD of Hafnium Oxide Thin Films from Tetrakis(ethylmethylamino)hafnium and Ozone,” *J. Electrochem. Soc.* **152**(3), G213 (2005).
- [28] Aarik, J., Aidla, A., Mändar, H., Uustare, T., “Atomic layer deposition of titanium dioxide from TiCl₄ and H₂O: investigation of growth mechanism,” *Appl. Surf. Sci.* **172**(1–2), 148–158 (2001).
- [29] Hennessy, J., Jewell, A. D., Greer, F., Lee, M. C., Nikzad, S., “Atomic layer deposition of magnesium fluoride via bis(ethylcyclopentadienyl)magnesium and anhydrous hydrogen fluoride,” *J. Vac. Sci. Technol. A* **33**(1), 01A125 (2015).
- [30] Hennessy, J., Balasubramanian, K., Moore, C. S., Jewell, A. D., Nikzad, S., France, K., Quijada, M., “Performance and prospects of far ultraviolet aluminum mirrors protected by atomic layer deposition,” *J. Astron. Telesc. Instruments, Syst.* **2**(4), 041206 (2016).
- [31] Pilvi, T., Ritala, M., Leskelä, M., Bischoff, M., Kaiser, U., Kaiser, N., “Atomic layer deposition process with TiF₄ as a precursor for depositing metal fluoride thin films,” *Appl. Opt.* **47**(13), C271-4 (2008).
- [32] Putkonen, M., Szeghalmi, A., Pippel, E., Knez, M., “Atomic layer deposition of metal fluorides through oxide chemistry,” *J. Mater. Chem.* **21**(38), 14461 (2011).
- [33] George, S. M., “Atomic layer deposition: an overview,” *Chem. Rev.* **110**(1), 111–131 (2010).
- [34] Szeghalmi, A., Helgert, M., Brunner, R., Heyroth, F., Gösele, U., Knez, M., “Atomic layer deposition of Al₂O₃ and TiO₂ multilayers for applications as bandpass filters and antireflection coatings,” *Appl. Opt.* **48**(9), 1727–1732 (2009).
- [35] Nikzad, S., Hoenk, M. E., Greer, F., Jacquot, B., Monacos, S., Jones, T. J., Blacksberg, J., Hamden, E., Schiminovich, D., et al., “Delta doped Electron-multiplied CCD with Absolute Quantum Efficiency over 50% in the near to far Ultraviolet Range for Single Photon Counting Applications,” *Appl. Opt.* **51**(3), 365–369 (2012).
- [36] Jewell, A. D., Hamden, E. T., Ong, H. R., Hennessy, J., Goodsall, T., Shapiro, C., Cheng, S., Jones, T., Carver, A., et al., “Detector performance for the FIREBall-2 UV experiment,” *Proc. SPIE - Int. Soc. Opt. Eng.* **9601** (2015).
- [37] Hamden, E. T., Lingner, N., Kyne, G., Morrissey, P., Martin, D. C., “Noise and dark performance for FIREBall-2 EMCCD delta-doped CCD detector,” *Proc. SPIE 9601 UV, X-Ray, Gamma-Ray Sp. Instrum. Astron. XIX*, O. H. Siegmund, S. R. McCandliss, C. Ertley, B. T. Fleming, J. C. Green, and A. Tremsin, Eds., 00:10, San Diego (2015).
- [38] Hamden, E. T., Jewell, A. D., Shapiro, C. A., Cheng, S. R., Goodsall, T. M., Hennessy, J., Hoenk, M. E., Jones, T. J., Gordon, S., et al., “Charge-coupled devices detectors with high quantum efficiency at UV wavelengths,” *J. Astron. Telesc. Instruments, Syst.* **2**(3), 036003 (2016).
- [39] Hennessy, J., Jewell, A. D., Hoenk, M. E., Nikzad, S., “Metal-Dielectric Filters for Solar-Blind Silicon Ultraviolet Detectors,” *Appl. Opt.* **54**(11), 3507–3512 (2015).
- [40] “TFCalc: Thin Film Design Software for Windows,” Version 3.5 (2009).
- [41] Edward D. Palik, ed., *Handbook of Optical Constants of Solids*, Academic Press, San Diego (1998).